SCIENTIFIC REPORTS

OPEN

SUBJECT AREAS:
COMPOSITES
METALS AND ALLOYS

Received
16 October 2014

Accepted
16 January 2015

Published
10 February 2015

Correspondence and requests for materials should be addressed to L.S.C. (lscui@cup.edu.cn); Y.N.L. (yinong.liu@uwa.edu.au) or X.D.L. (xl3p@virginia.edu)

A biopolymer-like metal enabled hybrid material with exceptional mechanical prowess

Junsong Zhang[1], Lishan Cui[1], Daqiang Jiang[1], Yinong Liu[2], Shijie Hao[1], Yang Ren[3], Xiaodong Han[4], Zhenyang Liu[1], Yunzhi Wang[5,6], Cun Yu[1], Yong Huan[7], Xinqing Zhao[8], Yanjun Zheng[1], Huibin Xu[8], Xiaobing Ren[5] & Xiaodong Li[9]

[1]State Key Laboratory of Heavy Oil Processing and Department of Materials Science and Engineering, China University of Petroleum, Beijing 102249, China, [2]School of Mechanical and Chemical Engineering, The University of Western Australia, Crawley, WA 6009, Australia, [3]X-ray Science Division, Argonne National Laboratory, Argonne, Illinois 60439, USA, [4]Institute of Microstructure and Properties of Advanced Materials, Beijing University of Technology, Beijing 100124, China, [5]State Key Laboratory for Mechanical Behavior of Materials and Frontier Institute of Science and Technology, Xi'an Jiaotong University, Xi'an 710049, China, [6]Department of Materials Science and Engineering, The Ohio State University, Columbus, OH 43210, USA, [7]State Key Laboratory of Nonlinear Mechanics (LNM), Institute of Mechanics, Chinese Academy of Sciences, Beijing 100190, China, [8]School of Materials Science and Engineering, Beihang University, Beijing 100191, China, [9]Department of Mechanical & Aerospace Engineering, University of Virginia, Charlottesville, Virginia 22904-4746, USA.

The design principles for naturally occurring biological materials have inspired us to develop next-generation engineering materials with remarkable performance. Nacre, commonly referred to as nature's armor, is renowned for its unusual combination of strength and toughness. Nature's wisdom in nacre resides in its elaborate structural design and the judicious placement of a unique organic biopolymer with intelligent deformation features. However, up to now, it is still a challenge to transcribe the biopolymer's deformation attributes into a stronger substitute in the design of new materials. In this study, we propose a new design strategy that employs shape memory alloy to transcribe the "*J*-curve" mechanical response and uniform molecular/atomic level deformation of the organic biopolymer in the design of high-performance hybrid materials. This design strategy is verified in a TiNi-Ti_3Sn model material system. The model material demonstrates an exceptional combination of mechanical properties that are superior to other high-performance metal-based lamellar composites known to date. Our design strategy creates new opportunities for the development of high-performance bio-inspired materials.

In the game of survival of the fittest, Nature, after millions of years of evolution, presents us with an abundance of rational designs of hierarchically structured materials of exceptional mechanical properties and functionalities that are still beyond the reach of many engineered materials. The design wisdom in these natural materials often inspires us to create and develop new and better man-made materials. Rigid biological materials are renowned for their remarkable mechanical robustness that often far exceeds what can be expected from a simple mixture of their components[1–4]. One of the best examples is nacre (mother-of-pearl), which is commonly referred to as nature's armors. Nacre possesses a hierarchical structure of surprising simplicity consisting of brittle inorganic aragonite (a mineral form of $CaCO_3$) platelets sandwiched with soft organic biopolymer layers[1–4]. The mineral component is in a layered form and serves as the primary load bearer for strength[2,4]. The soft organic biopolymer layers in-between play a critical role in both load distribution and energy dissipation due to its unique deformation features[2,4–6].

Macroscopically, the organic biopolymer responds to external mechanical loading in an intelligent manner (see Table 1 and Fig. 1a). It deforms at a low flow stress up to a large flow strain with a very low hardening effect (or high compliance), followed by a remarkably high strain-stiffening to reach a high ultimate rupture strength[4–6]. This deformation feature has been referred to as the "*J*-curve", in recognition of the shape of the stress-strain (or load-displacement) curve[4–6]. The coupling of low flow stress (point A in Fig. 1a) and large flow strain (A–B in Fig. 1a) renders the biopolymer "easy deformability", acting as a load distributor and deformation coordinator between the brittle mineral and biopolymer components, effectively reducing stress concentration[2,3]. The strain-stiffening at higher strain levels (B–C in Fig. 1a) effectively prevents excessive local deformation and instable

Table 1 | Comparison of biological materials and different engineering materials in macroscopic and microscopic characteristics. The organic biopolymer has a ''*J*-curve'' deformation feature, which is characterized by an increasing ''strain-hardening coefficient'', and a relatively uniform deformation mechanism on a molecular level. Some synthetic polymers exhibit similar features to the biopolymer, but show lack of strength. Conventional metallic materials have higher strengths than synthetic polymers. They deform primarily via dislocation movement, generally with a decreasing strain-hardening coefficient (lack of ''*J-curve*''). Shape memory alloys possess advantages of both the organic biopolymer and conventional metallic materials, including the ''*J-curve*'' deformation behavior, relatively uniform lattice deformation mechanism on the atomic level, and high strength

		Macroscopic feature		Microscopic feature
Materials		*J*-curve	High strength	Uniform microscopic deformation mechanism
Biological material	Organic biopolymer	√		√
Engineering material	Synthetic polymer	√		√
	Conventional metal		√	
	Shape memory alloy	√	√	√

"run-away" deformation, thus enabling the composite to achieve a higher ultimate strength[2,5]. Clearly, the biopolymer component "wisely" manages the deformation in the hierarchical architecture of nacre to prevent/delay catastrophic fracture[2,3,5].

Microscopically, the organic biopolymer undergoes these deformation stages through molecular reconfiguration, including uncoiling or straightening (the inset in Fig. 1a), in a uniform manner without introducing discrete structural defects (like dislocations in metals) piling-up at organic-inorganic interfaces[4,6]. This deformation mode uniformly distributes stress on a molecular/atomic level and expels stress concentration at organic-inorganic interfaces, thus assuring efficient load transfer to optimize the mechanical performance of the mineral component[6,7]. Obviously, the deformation mechanism of the organic biopolymer is microscopically favorable for enhancing the toughness and strength of nacre[4–6]. In this regard, apart from the structural design strategy, the unique "*J*-curve"-shaped mechanical response and the uniform, rigid-component-friendly molecular/atomic level microscopic deformation feature are two important design criteria in selecting substitute materials for the biopolymer in order to achieve nature's accomplishments in engineered composites.

Substantial efforts have been devoted to the synthesis of high-performance composite materials by reproducing the hierarchically layered structures of natural rigid biological materials[8–11]. Several techniques, such as tape or slip casting[12], layer-by-layer deposition[11,13], and freeze casting[9,10], have been used to synthesize bio-inspired composite materials. Previously, hard and brittle materials were chosen as the mineral component, whereas synthetic polymers or conventional soft metallic materials were selected as substitutes for the organic biopolymer component. One limitation of using synthetic polymers is their generally low strength (see Table 1)[11], which handicaps the mechanical performance of the composites. The use of metallic materials (see Table 1), which have relatively higher strengths than synthetic polymers, indeed improves the mechanical performance. However, these metallic materials do not exhibit "*J*-curve" deformation behavior (Fig. 1b). In addition, they deform by dislocation movement (the inset in Fig. 1b), which is nonuniform at the atomic scale[14]. As a result, conventional metallic materials fail to satisfy either of the two aforementioned design criteria.

A unique and promising choice, which has never been attempted in the past, is shape memory alloys (SMAs) (see Table 1 and Fig. 1c). Due to its thermoelastic martensitic transformation, a SMA exhibits

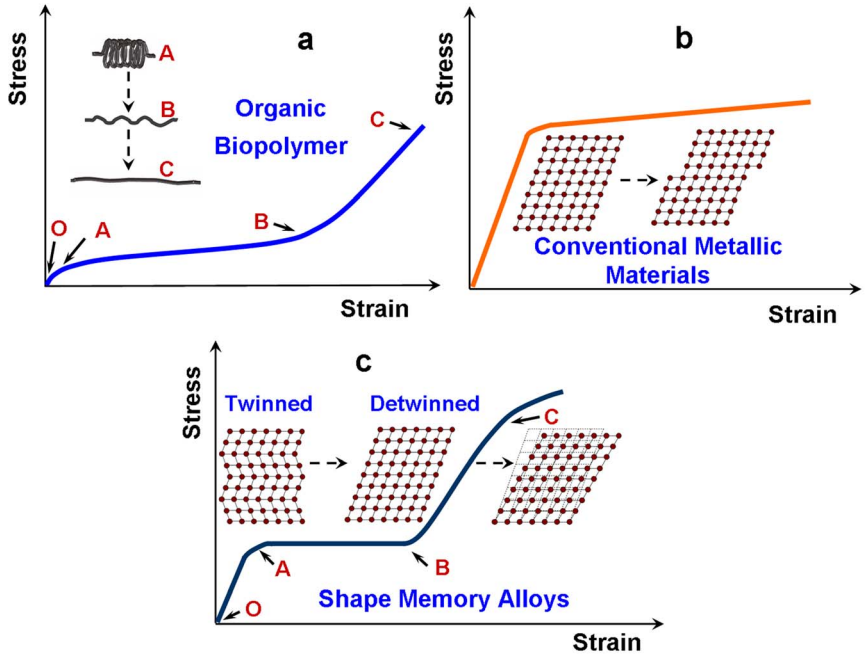

Figure 1 | Illustrative comparison of deformation behaviors and the mechanisms of three toughening components in the composites. (a) Organic biopolymer. (b) Conventional soft metallic materials. (c) Shape memory alloys. The insets schematically illustrate deformation mechanisms on the atomic/molecular level.

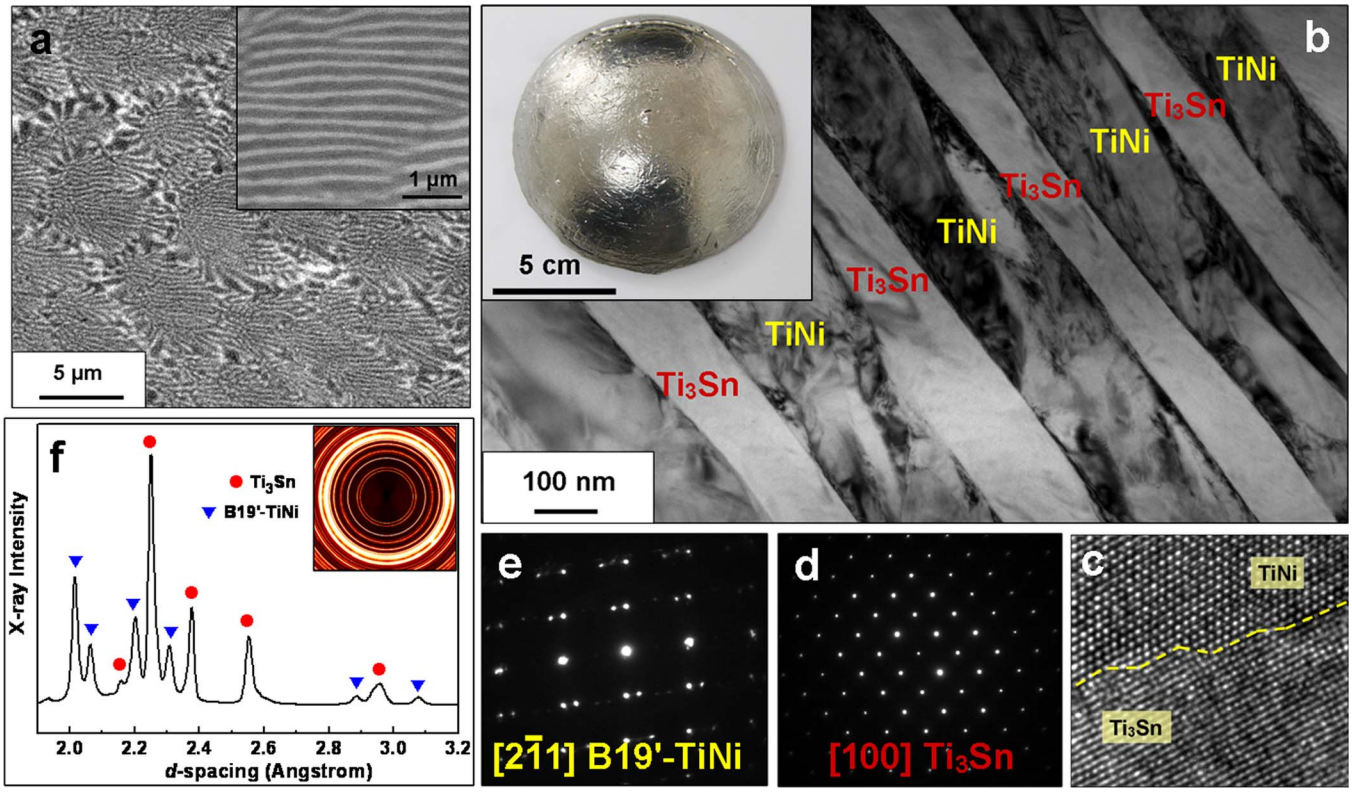

Figure 2 | Typical microstructure of the TiNi-Ti_3Sn composite. (a) Scanning electron microscopy backscattered electron images of the composite. The inset shows the Ti_3Sn (light)-TiNi (dark) lamellar structure at high magnification. (b) Transmission electron microscopy (TEM) bright-field image of the composite. The inset shows the button ingot of the composite. (c) High-resolution TEM image of the interface between TiNi and Ti_3Sn. (d) and (e) display selected-area electron diffraction patterns of the Ti_3Sn and TiNi lamellae, respectively, shown in Fig. 2b. (f) One-dimensional high-energy X-ray diffraction (HE-XRD) pattern of the composite. The inset contains its corresponding two-dimensional HE-XRD pattern.

a "*J*-curve" stress-strain behavior (Fig. 1c) through a relatively uniform lattice deformation mechanism (the inset in Fig. 1c and Supplementary Fig. 1)[15], which satisfies both design criteria for replicating the organic biopolymer. Upon loading, the SMA experiences a low stress yielding (point A in Fig. 1c) over a large strain (A–B in Fig. 1c) via either a stress-induced martensitic transformation (Supplementary Fig. 1) or martensite variant reorientation by detwinning (the inset in Fig. 1c). After that, the detwinned martensite rapidly stiffens with increasing strain (B–C in Fig. 1c), which is primarily related to its elastic deformation, to reach a high ultimate strength (point C in Fig. 1c). The second important characteristic of a SMA is the microscopic deformation mechanism. The stress-induced martensitic transformation (Supplementary Fig. 1) or detwinning of the martensite variants (the inset in Fig. 1a) is a relatively uniform lattice shear distortion with a maximum strain of ~10% (in TiNi)[15,16], which is fundamentally different from the dislocation slip in conventional metals (the inset in Fig. 1b). At a dislocation, the lattice distortion strain is highly localized and reaches to ~100%[14,16], which triggers large strain mismatch at the interface with the elastically deformed rigid component. The large strain mismatch in turn results in local stress concentration at the interfaces, thus inducing premature local failure of the rigid component. Conversely, the lattice shear distortion of the martensite is relatively uniform and is much easier to coordinate at the interface with the elastic distortion of the rigid component[16], which helps to prevent high local stress concentration and assure a relatively uniform stress distribution, thus preventing the premature failure of the rigid component. Therefore, SMAs endow a unique and promising opportunity for the design of high-performance bio-inspired engineering composite materials.

To verify this hypothesis, a brittle Ti_3Sn intermetallic compound with a high damping capacity[17,18] was selected to replicate the inorganic mineral component, and a TiNi SMA was employed to mimic the organic biopolymer. This design is supported by the fact that the TiNiSn system undergoes a eutectic solidification of TiNi–Ti_3Sn to form an in situ submicron laminar composite. In this study, TiNi–Ti_3Sn eutectic composite ingots with a chemical composition of $Ti_{57}Ni_{35}Sn_8$ (at. %) were prepared using coupled arc melting and directional solidification techniques. Fig. 2 presents a typical microstructural analysis of the composite. The microstructure consists of fine composite lamellae of TiNi and Ti_3Sn (Figs. 2a and 2b) with well-bonded interfaces (Fig. 2c). Selected-area electron diffraction patterns, which were obtained from the bright layer and gray layer (Fig. 2b), confirm the D019-Ti_3Sn (Fig. 2d) structure and B19'-TiNi (Fig. 2e) structure, respectively. This observation is consistent with high-energy X-ray diffraction measurements (Fig. 2f). The thicknesses of the TiNi layer and Ti_3Sn layer are approximately 300 nm and 200 nm, respectively. The directional solidification process helped to re-arrange the TiNi and Ti_3Sn alternating layers in one direction (Supplementary Fig. 2).

To uncover the mechanical response of the TiNi component in the composite, in situ synchrotron high-energy X-ray diffraction (HE-XRD) measurements were performed during compressive deformation (Supplementary Fig. 3)[16,19,20]. The evolutions of the lattice strains (indicating elastic strains) of TiNi and Ti_3Sn in the loading direction as a function of the applied macroscopic strain are shown in Fig. 3a and Supplementary Fig. 4. Fig. 3a illustrates that as the applied strain increased, the lattice strain of TiNi initially increased linearly (O-A), and then remained almost constant at 0.7% to approximately 4% of the applied strain (A–B) before increased rapidly again at higher applied strains (B–C). The TiNi lattice strain reached 1.1% at 9% of applied strain, beyond which the TiNi lattice strain continued to increase at a reduced rate to a maximum of 1.5% (C–D). This mech-

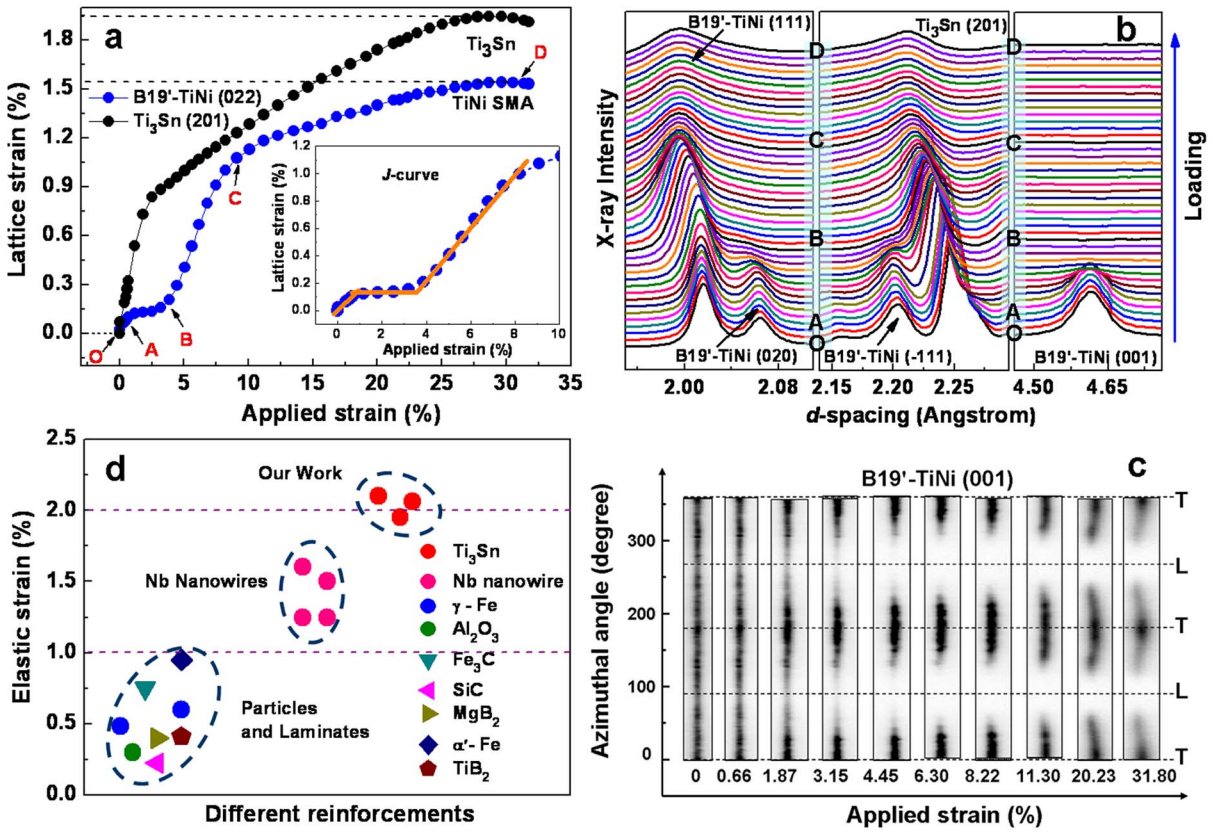

Figure 3 | Deformation behavior of the TiNi-Ti_3Sn composite. (a) The lattice strain evolutions of B19'-TiNi (022) and Ti_3Sn (201) planes perpendicular to the loading direction as a function of the applied macroscopic strain. The inset shows an enlarged view of the lattice strain curve of the TiNi in the initial stages of deformation. (b) The evolution of the diffraction spectrum of the composite during compression in three sections, which reveals B19'-TiNi (111), B19'-TiNi (020), B19'-TiNi ($\bar{1}11$), B19'-TiNi (001), and Ti_3Sn (201) peaks in the direction perpendicular to the loading direction. (c) The azimuthally (0 to 360°) unrolled diffraction patterns of B19'-TiNi (001) at different applied strains. The curvature of the diffraction lines indicates the stress state of the sample. The transverse direction (T) experienced minimum compression, and the longitudinal direction (L) experienced maximum compression. The change in diffraction intensity along the azimuthal angle originates from the martensite variant reorientation by detwinning. (d) The comparison of the elastic strains of Ti_3Sn achieved in our composite with different reinforcements (such as nanowires, laminates, and particles) embedded in conventional metal matrices, which are deformed by dislocation slip [blue circle[21], olive circle[22], dark cyan downtriangle[23], magenta lefttri[24], dark yellow righttri[25], navy diamond[26], wine pentagon[27], pink circle[28,29]].

anical response exhibits a "*J-shaped*" curve between the lattice strain and the applied strain (the inset in Fig. 3a). Considering that the stress endured by the TiNi can be directly converted from its elastic lattice strain via Young's modulus, the "*J*-shaped" lattice strain versus the applied strain curve explicitly implies a "*J*-shaped" stress versus the applied strain curve of the TiNi in the composite. The elastic strain at the yield (point A in Fig. 3a) and the maximum elastic strain (point D in Fig. 3a) of the TiNi component in the composite are 0.15% and 1.5%, respectively. Using E = 50 GPa for TiNi[15], the strengths that correspond to points A and D are estimated to be 75 and 750 MPa, respectively, which are approximately three to 10 times greater than the strengths of the organic biopolymer in natural rigid biological materials[4].

The microscopic deformation mechanism of the TiNi component during loading was analyzed by in situ synchrotron HE-XRD measurements. Fig. 3b shows the evolution of the diffraction spectrum recorded in the loading direction (refer to Supplementary Fig. 3, Φ = 90°). The pristine TiNi was in a B19' martensitic state, as evidenced by the B19'-TiNi (020), ($\bar{1}11$), (001), and (111) diffraction peaks. Labels "A"-"D" on the side in Fig. 3b correspond to the labels marked on the lattice strain curve of TiNi shown in Fig. 3a. Upon loading, the diffraction intensity of the (111) peak increased as the diffraction intensities of the (020), ($\bar{1}11$), and (001) peaks decreased, indicating martensite variant reorientation by detwinning. Additional evidence of the TiNi martensite variant reorientation by detwinning is shown in Fig. 3c and Supplementary Fig. 5. The detwinning deformation process of TiNi is proceeded by a relatively uniform lattice shear distortion of the martensite[15].

The elastic strain (lattice strain) of Ti_3Sn (Fig. 3a) in the loading direction rapidly increased during the stages corresponding to the initial elastic deformation and the detwinning of the TiNi, and then continued to increase at a slower rate up to 2% (Fig. 3a), which is more than six times the elastic strain of free-standing Ti_3Sn (approximately 0.3%)[17]. This value is also significantly superior to the elastic strains of other reinforcements (such as nanowires, laminates, and particles) embedded in conventional metal matrices that deform by dislocation slip, as demonstrated in Fig. 3d[21–29]. A high lattice elastic strain implies high elastic stress. Using E = 207 GPa for Ti_3Sn[30], the lattice elastic stress, which is endured locally by the Ti_3Sn in the composite, is estimated to be 4,100 MPa. This suggests that the Ti_3Sn is the main load bearer and significantly contributes to the strength of the composite. Such high elastic strain and outstanding load-bearing capability of Ti_3Sn in the composite may be attributed to the uniform martensite lattice distortion mechanism of the TiNi component and its "*J*-curve" deformation behavior.

It has been demonstrated recently that nanomaterials can exhibit ultra-large elastic strains when embedded in martensitic phase transforming matrix owing to the principle of lattice strain matching, in

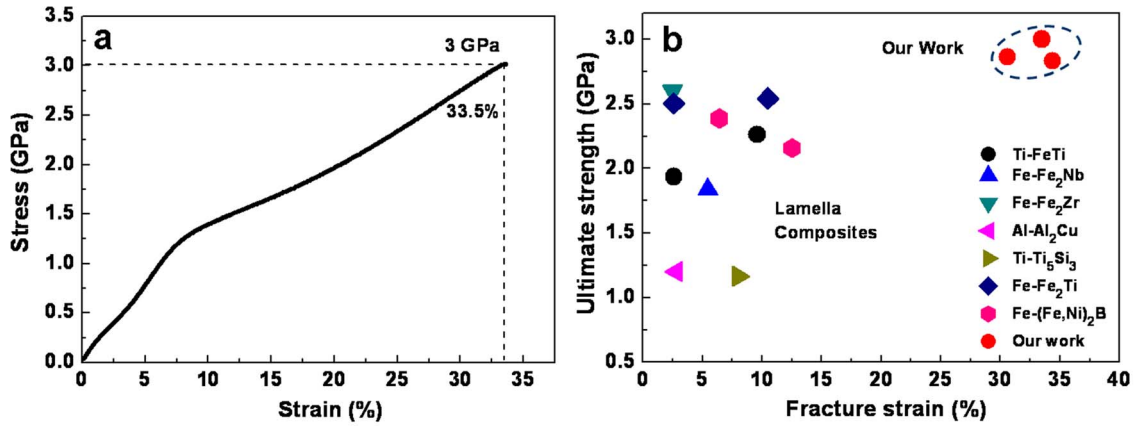

Figure 4 | Mechanical properties of the TiNi-Ti_3Sn composite. (a) Room-temperature compressive stress–strain curve of the composite. (b) Comparison of the mechanical properties of our composite with those of other high-performance metal-based lamellar composites in which the soft component is a conventional metal (without the "*J*-curve" deformation attributes) rather than the biopolymer-like metal ("*J*-curve" deformation attributes) [black circle[31], blue uptriangle[32], dark cyan downtriangle[33], magenta lefttri[34], dark yellow righttri[35], navy diamond[36], pink hexagon[37]].

clear contrast to matrices that deform by dislocation slip[16]. Martensitic transformation of the TiNi matrix is a process of uniform lattice distortion with a shear strain of typically several percent, which is compatible to the uniform elastic strains of Ti_3Sn, thus allowing effective strain coupling between the two. In contrast, in a matrix that deforms by dislocation slip, the lattice strain is highly non-uniform at the atomic level, being ~100% at the site of a dislocation line and well below 1% (the yield elastic strain) elsewhere away from dislocation lines. Such lattice strain distribution is highly incompatible to the uniform elastic stain of the reinforcement (Ti_3Sn in this case), preventing effective load transfer and achievement of large elastic strains of the reinforcement.

To achieve large elastic strains, so to harness the intrinsic strength of the load bearing component, it is also essential for the composite to have an effective load distribution mechanism, so to avoid local stress concentration and local failure. This is achieved by the "*J*-curve" behavior of the TiNi. The low flow stress and large flow strain of the *J*-curve (in the 'toe' and 'heel' regions) enable TiNi shape memory alloy to act as a load distributor and deformation coordinator among the brittle Ti_3Sn lamellae, maximizing the load baring capability of the composite. The strong strain-stiffening at higher strain levels of the *J*-curve (the 'ankle' region and above) stops excessive local deformation and forces initiation of new deformation sites elsewhere, thus spreading the deformation over large volumes throughout the composite. This mechanism effectively prevents instable "run-away" deformation and premature local failure, thus enabling the composite to achieve optimum ultimate strength.

The mechanical properties of our TiNi-Ti_3Sn composite are shown in Fig. 4, Supplementary Fig. 6. The composite exhibits a maximum ultimate compressive strength of 3 GPa and a large fracture strain that exceeds 30%, which are superior to the ultimate compressive strengths and fracture strains of other high-performance metal-based lamellar composites in which the soft component is a conventional metal (without the "*J*-curve" deformation attributes) rather than the biopolymer-like metal ("*J*-curve" deformation attributes) (Fig. 4b)[31–37]. In addition, the composite also exhibits a high damping capacity ($Q^{-1} > 10^{-2}$) at low frequencies (Supplementary Fig. 7), which is comparable to the damping capacity of commercial Mn-Cu high-damping alloys[38], and ultrasonic attenuation (Supplementary Fig. 8). The high-damping capacity primarily originates from the movement of twin boundaries in the Ti_3Sn[30] and TiNi[15] components.

In this work, by cementing a TiNi shape memory alloy with a brittle Ti_3Sn intermetallic compound into an in situ lamellar composite structure through eutectic solidification, we have demonstrated a feasible design strategy for developing high-performance bio-inspired bulk materials. The design is based on transcribing the principles of the unique "*J*-curve" mechanical response and the uniform molecular/atomic level microscopic deformation of the organic biopolymer by shape memory alloy. This strategy presents a new promise for the design and synthesis of bio-inspired engineering materials to achieve exceptionally high mechanical robustness for applications in an extensive range of fields.

Methods

Alloy ingots with a nominal composition of $Ti_{57}Ni_{35}Sn_8$ (at. %) were prepared by arc melting in a water-cooled copper hearth in an argon atmosphere. The raw materials used were of commercial purity Ti (99.99 wt. %), Ni (99.99 wt. %), and Sn (99.99 wt. %). The ingot was solidified via a directional solidification process, which was performed in a laboratory-scale Bridgman-type directional solidification furnace (LMC, liquid metal cooling technology) with a 30 mm/min drawing velocity.

The microstructure and chemical composition of the composite were analyzed using a FEI Tecnai G2 F20 transmission electron microscope (TEM), which was equipped with an energy dispersive X-ray spectroscopic analyzer operated at 200 kV. The morphology of the composite was characterized using a FEI-200F scanning electron microscope (SEM) operated at 20 kV.

The compression properties of the composite were tested using a servo-hydraulic materials testing system (MTS 810) at room temperature at a strain rate of 5×10^{-4} s^{-1}. Cylindrical compression samples with a diameter of 5 mm and a length of 10 mm were prepared according to American Society for Testing and Materials (ASTM) standards.

The damping capacity of the composite was measured using a dynamic mechanical analyzer (DMA Q800, TA) in single cantilever mode. The geometry of the damping specimens was $1 \times 4 \times 40$ mm^3. Damping tests were conducted at a frequency of 1 Hz in the temperature range of −130°C to 300°C with a constant heating/cooling rate of 5°C/min. Ultrasonic attenuation was measured in pulse-echo mode of a longitudinal wave using 2 MHz transducers. The ultrasonic attenuation samples were 30 mm in diameter and 30 mm in long.

In situ synchrotron high-energy X-ray diffraction (HEXRD) measurements were performed during the compression test on beamline 11-ID-C at the Advanced Photon Source, Argonne National Laboratory, USA. High-energy X-rays with an energy of 115 keV, a beam size of 0.6×0.6 mm^2 and a wavelength of 0.10798 Å were used to obtain two-dimensional (2D) diffraction patterns in the transmission configuration. Gaussian fits were employed to determine the positions of the diffraction peaks. The lattice strain for the reflection peak is calculated using $|d_{hkl}\text{-}d_{hkl}^0|/d_{hkl}^0$, where d_{hkl}^0 is the "unstressed" lattice parameter (i.e., the peak position at zero applied stress). The error of the lattice strain measurements was less than 0.05%.

1. Mayer, G. Rigid Biological Systems as Models for Synthetic Composites. *Science* **310**, 1144–1147 (2005).
2. Espinosa, H. D., Rim, J. E., Barthelat, F. & Buehler, M. J. Merger of structure and material in nacre and bone – Perspectives on de novo biomimetic materials. *Prog. Mater Sci.* **54**, 1059–1100 (2009).
3. Wang, R. Z. & Gupta, H. S. Deformation and Fracture Mechanisms of Bone and Nacre. *Annu. Rev. Mater. Res.* **41**, 41–73 (2011).
4. Chen, P. Y., McKittrick, J. & Meyers, M. A. Biological materials: Functional adaptations and bioinspired designs. *Prog. Mater Sci.* **57**, 1492–1704 (2012).

5. Xu, Z. H. & Li, X. D. Deformation Strengthening of Biopolymer in Nacre. *Adv. Funct. Mater.* **21**, 3883–3888 (2011).
6. Smith, B. L. *et al.* Molecular mechanistic origin of the toughness of natural adhesives, fibres and composites. *Nature* **399**, 761–763 (1999).
7. Wang, R. Z., Suo, Z. G., Evans, A., Yao, N. & Aksay, I. Deformation mechanisms in nacre. *J. Mater. Res* **16**, 2485–2493 (2001).
8. Clegg, W. J., Kendall, K., Alford, N. M., Button, T. & Birchall, J. A simple way to make tough ceramics. *Nature* **347**, 455–457 (1990).
9. Deville, S., Saiz, E., Nalla, R. K. & Tomsia, A. P. Freezing as a Path to Build Complex Composites. *Science* **311**, 515–518 (2006).
10. Munch, E. *et al.* Tough, Bio-Inspired Hybrid Materials. *Science* **322**, 1516–1520 (2008).
11. Bonderer, L. J., Studart, A. R. & Gauckler, L. J. Bioinspired Design and Assembly of Platelet Reinforced Polymer Films. *Science* **319**, 1069–1073 (2008).
12. Moya, J. S. Layered ceramics. *Adv. Mater.* **7**, 185–189 (1995).
13. Podsiadlo, P. *et al.* Ultrastrong and stiff layered polymer nanocomposites. *Science* **318**, 80–83 (2007).
14. Ogata, S., Li, J. & Yip, S. Ideal pure shear strength of aluminum and copper. *Science* **298**, 807–811 (2002).
15. Otsuka, K. & Ren, X. Physical metallurgy of Ti–Ni-based shape memory alloys. *Prog. Mater Sci.* **50**, 511–678 (2005).
16. Hao, S. *et al.* A Transforming Metal Nanocomposite with Large Elastic Strain, Low Modulus, and High Strength. *Science* **339**, 1191–1194 (2013).
17. Hashimoto, T., Nakamura, M. & Takeuchi, S. Plastic deformation of Ti_3Sn. *Mater. Trans., JIM* **31**, 195–199 (1990).
18. Vdovychenko, O., Bulanova, M., Fartushna, Y. V. & Shcheretsky, A. Dynamic mechanical behavior of intermetallic Ti_3Sn. *Scr. Mater.* **62**, 758–761 (2010).
19. Jiang, D. Q. *et al.* In situ synchrotron investigation of the deformation behavior of nanolamellar Ti_5Si_3/TiNi composite. *Scr. Mater.* **78**, 53–56 (2014).
20. Young, M. L., Wagner, M. F. X., Frenzel, J., Schmahl, W. W. & Eggeler, G. Phase volume fractions and strain measurements in an ultrafine-grained NiTi shape-memory alloy during tensile loading. *Acta Mater.* **58**, 2344–2354 (2010).
21. Muránsky, O., Šittner, P., Zrník, J. & Oliver, E. C. In situ neutron diffraction investigation of the collaborative deformation–transformation mechanism in TRIP-assisted steels at room and elevated temperatures. *Acta Mater.* **56**, 3367–3379 (2008).
22. Roy, S., Gibmeier, J. & Wanner, A. In situ Study of Internal Load Transfer in a Novel Metal/Ceramic Composite Exhibiting Lamellar Microstructure Using Energy Dispersive Synchrotron X-ray Diffraction. *Adv. Eng. Mater.* **11**, 471–477 (2009).
23. Young, M. L., Almer, J. D., Daymond, M. R., Haeffner, D. R. & Dunand, D. C. Load partitioning between ferrite and cementite during elasto-plastic deformation of an ultrahigh-carbon steel. *Acta Mater.* **55**, 1999–2011 (2007).
24. Wilkes, T. E., Harder, B. J., Almer, J. D. & Faber, K. T. Load partitioning in honeycomb-like silicon carbide aluminum alloy composites. *Acta Mater.* **57**, 6234–6242 (2009).
25. Young, M. L., DeFouw, J., Almer, J. D. & Dunand, D. C. Load partitioning during compressive loading of a Mg/MgB_2 composite. *Acta Mater.* **55**, 3467–3478 (2007).
26. Jia, N. *et al.* An in situ high-energy X-ray diffraction study of micromechanical behavior of multiple phases in advanced high-strength steels. *Acta Mater.* **57**, 3965–3977 (2009).
27. Bacon, D. H., Edwards, L., Moffatt, J. E. & Fitzpatrick, M. E. Synchrotron X-ray diffraction measurements of internal stresses during loading of steel-based metal matrix composites reinforced with TiB_2 particles. *Acta Mater.* **59**, 3373–3383 (2011).
28. Aydıner, C., Brown, D., Mara, N., Almer, J. & Misra, A. In situ x-ray investigation of freestanding nanoscale Cu–Nb multilayers under tensile load. *Appl. Phys. Lett.* **94**, 031906-031906-3 (2009).
29. Thilly, L. *et al.* A new criterion for elasto-plastic transition in nanomaterials: Application to size and composite effects on Cu–Nb nanocomposite wires. *Acta Mater.* **57**, 3157–3169 (2009).
30. Wong, C. R. & Fleischer, R. L. Low frequency damping and ultrasonic attenuation in Ti_3Sn-based alloys. *J. Mater. Res.* **9**, 1441–1448 (1994).
31. Das, J., Kim, K. B., Baier, F., Loser, W. & Eckert, J. High-strength Ti-base ultrafine eutectic with enhanced ductility. *Appl. Phys. Lett.* **87**, 161907-161907-3 (2005).
32. Park, J. M. *et al.* High strength ultrafine eutectic Fe–Nb–Al composites with enhanced plasticity. *Intermetallics* **16**, 642–650 (2008).
33. Park, J. M. *et al.* Nanostructure–dendrite composites in the Fe–Zr binary alloy system exhibiting high strength and plasticity. *Scr. Mater.* **57**, 1153–1156 (2007).
34. Park, J. M. *et al.* High-strength bulk Al-based bimodal ultrafine eutectic composite with enhanced plasticity. *J. Mater. Res.* **24**, 2605–2609 (2009).
35. Hu, Z., Zhan, Y. & She, J. The role of Nd on the microstructural evolution and compressive behavior of Ti–Si alloys. *Mater. Sci. Eng., A* **560**, 583–588 (2013).
36. Park, J. M. *et al.* Influence of heterogeneities with different length scale on the plasticity of Fe-base ultrafine eutectic alloys. *J. Mater. Res.* **23**, 2003–2008 (2008).
37. Pi, D. H. *et al.* Effect of Nb on microstructure and mechanical properties of ultrafine eutectic Fe–Ni–B–Si composites. *J. Alloys Compd.* **504S**, S487–S490 (2010).
38. Tian, Q., Yin, F., Sakaguchi, T. & Nagai, K. Internal friction behavior of twin boundaries in tensile-deformed Mn–15 at.% Cu alloy. *Mater. Sci. Eng., A* **442**, 433–438 (2006).

Acknowledgments

We thank Q. Zhou, J. X. Wei, X. B. Shi, S. Guo, and Q. K. Meng for valuable discussions on the damping capacity and deformation mechanism of the composite. This work is supported by the key program project of National Natural Science Foundation of China (NSFC) (51231008), the National 973 programs of China (2012CB619400), the NSFC (51071175), Australian Research Council (Grant No. DP140103805), and Foundation for Innovative Research Groups of the NSFC (Grant No. 51221163). Y. W. acknowledges support by National Basic Research Program of China (Grants Nos. 2012CB619402, 2014CB644003) and U.S. Natural Science Foundation DMR-1410322. Use of the Advanced Photon Source is supported by the U.S. Department of Energy, Office of Science, under contract no. DE-AC02-06CH11357.

Author contributions

L.C., Y.L. and X.L. designed the project. J.Z. carried out materials preparation and mechanical properties testing. Y.R. designed and supervised the synchrotron experiments. S.H. and C.Y. carried out the synchrotron experiments. D.J. and Z.L. carried out the SEM and TEM experiments. X.H., Y.Z. and X.R. supervised the analysis of deformation mechanism. Y.H. supervised the mechanical properties testing. X.Z. and H.X. supervised the materials preparation. J.Z., L.C., Y.L. and D.J. wrote the initial drafts of the manuscripts. X.L., Y.L., L.C., Y.W., X.H. and J.Z. wrote the final version of the manuscript.

Additional information

Supplementary information accompanies this paper at http://www.nature.com/scientificreports

Competing financial interests: The authors declare no competing financial interests.

How to cite this article: Zhang, J. *et al.* A biopolymer-like metal enabled hybrid material with exceptional mechanical prowess. *Sci. Rep.* **5**, 8357; DOI:10.1038/srep08357 (2015).